

Supporting Information

Polymorphic Solvates, Ionic-cocrystals and C-N Bond Formation to Form Ionic Cocrystal In Sulfamethoxazole and Sulfathiazole Derived Urea

Jitendra Nath, Jubaraj B. Baruah*

Content list

Title
Synthesis and characterization of the hosts, solvates, cocrystals and salts
Scheme S1: A plausible mechanism of the C-N bond formation from reaction of HSTZU with TBAI.
Table S1: Hydrogen bond parameters of solvates, cocrystals and salt
Table S2: Torsion angles of solvates, ionic cocrystals and salts of HSMZU
Table S3: Torsion angles of solvates of HSTZU
Figure S1: ORTEP diagram of HSMZU.DMF-P1 drawn with 50 % ellipsoid probability.
Figure S2: Powder X-ray diffraction patterns of the HSMZU.DMF-P1
Figure S3: FT-IR spectrum (neat) of the HSMZU.DMF-P1
Figure S4: ¹ H NMR (DMSO-d ₆ , 600 MHz) spectra of the HSMZU.DMF-P1
Figure S5: ¹ H NMR (DMSO-d ₆ , 600 MHz) spectra of the HSMZU
Figure S6: ¹ H-2D-HOMOCOSY (600 MHz, DMSO-d ₆) spectrum of the HSMZU.DMF-P1
Figure S7: ¹³ C NMR (125 MHz, DMSO-d ₆) spectra of the HSMZU
Figure S8: ¹³ C NMR (125 MHz, DMSO-d ₆) spectra of the HSMZU.DMF-P1
Figure S9: ¹ H NMR (DMSO-d ₆ , 600 MHz) spectra of the HSMZU.DMF-P1 at variable temperatures
Figure S10: Variable temperature ¹ H NMR spectra (DMSO-d ₆ , 600 MHz) of HSMZU.DMF-P1 with 10 equivalent of TBAI (* assignment of peaks)
Figure S11: ¹ H NMR (600 MHz, DMSO-d ₆) titration of HSMZU.DMF-P1 by adding different amounts of tetrabutylammonium (a) chloride and (b) bromide (showing the aromatic protons of HSMZU.DMF-P1)
Figure S12: ORTEP diagram of HSMZU.DMF-P2 drawn with 50% ellipsoid probability
Figure S13: Powder X-ray diffraction patterns of the HSMZU.DMF-P2
Figure S14: FT-IR spectrum (neat) of the HSMZU.DMF-P2
Figure S15 : Hirshfeld surfaces of (d) HSMZU.DMF-P1, (e) HSMZU.DMF-P2, (f) TBA(SMZU).
Figure S16: ORTEP diagram of TBA(SMZU) drawn with 50% ellipsoid probability
Figure S17: Powder X-ray diffraction patterns of the TBA(SMZU)
Figure S18: FT-IR spectrum (neat) of the TBA(SMZU)
Figure S19: ¹ H 2D-HOMOCOSY (600 MHz, DMSO-d ₆) spectrum of the TBA(SMZU)
Figure S20: ¹ H NMR (DMSO-d ₆ , 600 MHz) spectra of the TBA(SMZU).
Figure S21: ORTEP diagram of butyl-SMZU.TBAI drawn with 50% ellipsoid probability.
Figure S22: Powder X-ray diffraction patterns of the butyl-SMZU.TBAI
Figure S23: FT-IR spectrum (neat) of the butyl-SMZU.TBAI
Figure S24: ¹ H NMR (DMSO-d ₆ , 600 MHz) spectra of the butyl-SMZU.TBAI
Figure S25: ¹³ C NMR (125 MHz, DMSO-d ₆) spectra of the butyl-SMZU.TBAI.
Figure S26: ESI mass spectrum of the butyl-SMZU.
Figure S27: ORTEP diagram of HSTZU.DMF drawn with 50% ellipsoid probability
Figure S28: Powder X-ray diffraction patterns of the HSTZU.DMF
Figure S29: FT-IR spectrum (neat) of the HSTZU.DMF
Figure S30: ¹ H NMR (DMSO-d ₆ , 600 MHz,) spectra of the HSTZ.DMF

Figure S31: ^{13}C NMR (125 MHz, DMSO-d_6) spectra of the **HSTZ.DMF**

Figure S32: ^1H NMR (600 MHz, DMSO-d_6) titration showing the aromatic protons of **HSTZU.DMF** recorded by adding different amounts of tetrabutylammonium (a) chloride and (b) bromide

Figure S33: ORTEP diagram of **HSTZU.DMSO** drawn with 50% ellipsoid probability.

Figure S34: Powder X-ray diffraction patterns of the **HSTZU.DMSO**

Figure S35: FT-IR spectrum (neat) of the **HSTZU.DMSO**

Figure S36: ^1H 2D-HOMOCOSY (600 MHz, DMSO-d_6) spectrum of the **HSTZU.DMSO**

Figure S37: ^1H NMR (DMSO-d_6 , 600 MHz,) spectra of the **HSTZU.DMSO**

Figure S38: ^{13}C NMR (125 MHz, DMSO-d_6) spectra of the **HSTZU.DMSO**

Figure S39: ORTEP diagram of **HSTZU.TBAI** drawn with 50 % ellipsoid probability.

Figure S40: Powder X-ray diffraction patterns of the **HSTZU.TBAI**.

Figure S41: ^1H NMR (DMSO-d_6 , 600 MHz) spectra of the **HSTZU.TBAI**

Figure S42: ^{13}C NMR (125 MHz, DMSO-d_6) spectra of the **HSTZU.TBAI**

Figure S43: FT-IR spectrum (neat) of the **TBA(STZU)**

Figure S44: ^1H 2D-HOMOCOSY (600 MHz, DMSO-d_6) spectrum of the **TBA(STZU)**.

Figure S45: ^1H NMR (DMSO-d_6 , 600 MHz) spectra of the **TBA(STZU)**

Figure S46: ^{13}C NMR (125 MHz, DMSO-d_6) spectra of the **TBA(STZU)**

Figure S47: Thermogram of the polymorph (a) **HSMZU.DMF-P1** (b) **HSMZU.DMF-P2**

Figure S48: Differential scanning calorimetry of (a) **HSTZU.DMF** (b) **HSTZU.DMSO** (heating rate $10^\circ\text{C}/\text{min}$ under nitrogen atmosphere) .

Figure S49: Hirshfeld surfaces of (a) **HSTZU.DMF** (b) **HSTZU.DMSO**, (c) **HSTZU.TBAI**

Figure S50: Percentages of the $\text{H}\cdots\text{C}$, $\text{H}\cdots\text{H}$, $\text{H}\cdots\text{O}$, $\text{H}\cdots\text{N}$, $\text{H}\cdots\text{S}$ and $\text{H}\cdots\text{anion}$ interaction (include reciprocal contacts) in 2D fingerprint plots

Figure S51: 2D fingerprint plots (including reciprocal contacts) of the $\text{H}\cdots\text{C}$, $\text{H}\cdots\text{H}$, $\text{H}\cdots\text{O}$, $\text{H}\cdots\text{N}$ and $\text{H}\cdots\text{anion}$ interactions of a) **HSMZU.DMF-P1** b) **HSMZU.DMF-P2** c) **TBA(SMZU)**.

Figure S52: 2D fingerprint plots (including reciprocal contacts) of the $\text{H}\cdots\text{C}$, $\text{H}\cdots\text{H}$, $\text{H}\cdots\text{O}$, $\text{H}\cdots\text{N}$ and $\text{H}\cdots\text{anion}$ interactions of (a) **HSTZU.DMF** (b) **HSTZU.DMSO** (c) **HSTZU.TBAI**

Figure S53: Changes in the UV–visible spectra of (a) **HSTZU** and (b) **HSMZU** (3.3×10^{-5} M, 2mL in each case) in dimethylsulfoxide by aliquots (30 μL) of tetrabutylammonium fluoride (10^{-2} M)

Figure S54: Visual color change of a) **HSMZU** b) **STZU** after addition of **TBAF** and **TBABr** respectively.

Figure S55: HOMO and LUMO gap (a) **HSMZU.DMF-P1** (b) **HSMZU.DMF-P2** (c) **TBA(SMZU)**, (d) **HSTZU.DMF** (e) **HSMZU-P1** (f) **HSMZU-P2** (g) dimer of **HSMZU-P1** (h) dimer of **HSMZU-P2** (i) dimer of **TBA(SMZU)** (j) dimer of **HSTZU.DMF** (k) **HSMZU.DMSO** calculated by DFT using B3LYP/6-31+G (d, p) as basis set

Synthesis and characterization of the hosts, solvates, cocrystals and salts:

HSMZU.DMF-P1: A solution of 4-nitrophenylisocyanate (328 mg, 2 mmol) and sulfamethoxazole (507 mg, 2 mmol) in acetonitrile (30 ml) was refluxed for 2 hs after which the reaction mixture was stirred at room temperature for about 6 hs. This had resulted in the formation of a yellow precipitate. This precipitate was filtered and it was dissolved in 3 ml DMF.

The solution thus prepared was kept undisturbed, which provided the crystals of **HSMZU.DMF-P1** yield = 76 %. IR (Neat, cm^{-1}): 3272 (w), 3135 (w) 1724 (s), 1657 (s), 1615 (s), 1590 (s), 1574 (s), 1542 (s), 1495 (s), 1468 (s), 1409 (s), 1374 (s), 1384 (s), 1333 (m), 1317(s), 1251 (s), 1197 (s), 1162 (s), 1106 (s), 1091 (s), 1028 (m), 928 (s), 885 (s), 854 (s), 843 (m), 831 (s), 751 (s), 715 (s), 667 (s), 645 (s), 579 (s), 556 (s). ^1H NMR (600 MHz, DMSO-d_6 , ppm): 11.31 (s, 1H), 9.57 (s, N-H), 9.39 (s, N-H), 8.21- 8.20 (d, $J = 10$ Hz, 2H), 7.95 (s, 1H), 7.79 (d, $J = 8$ Hz), 7.70 (d, $J = 9$ Hz), 7.67 (d, $J = 8$ Hz), 6.13 (s, 1H), 2.89 (s, 3H), 2.73 (s, 3H), 2.29 (s, 3H). ^{13}C NMR (125 MHz, DMSO-d_6): 170.3, 162.3, 157.6, 151.8, 145.9, 143.6, 141.4, 132.3, 128.2, 125.2, 118.2, 117.8, 95.4, 35.8, 30.7, 12.1.

HSMZU.DMF-P2: A solution of the crude yellow precipitate of **SMZU** (103 mg, 0.25 mmol) was dissolved in DMF (10 ml) was stirred at 80°C for about 1 h. The solution was filtered to discard suspended material (if any) and it was kept undisturbed for crystallization. Upon standing for 8-10 days red block crystals of the **HSMZU.DMF-P2** were obtained (yield 82 %). IR (Neat, cm^{-1}): 3358 (s), 1719 (s), 1657 (s), 1618 (s), 1593 (s), 1557 (w), 1572 (s), 1538 (s), 1495 (s), 1441 (m), 1406 (s), 1376 (s), 1326 (s), 1304 (w), 1249 (s), 1198 (s), 1177 (m), 1163 (s), 1108 (s), 1092 (m), 1040 (s), 924 (m), 875 (s), 854 (s), 833 (s), 812 (s), 752 (s), 702 (s), 666 (s), 643 (s), 574 (s), 556 (s).

TBA(SMZU) Salt: The crude **HSMZU** (42 mg, 0.1 mmol) was dissolved in DMF (5 ml). To this solution TBAF trihydrate (63 mg, 0.2 mmol) was added and stirred for 30 mins. The solution was filtered and kept for crystallization, which yielded crystalline **TBA(SMZU)**. The crystals were decanted and characterized (yield 85 %). IR (Neat cm^{-1}): 2959 (s), 2874 (s), 1719 (s), 1609 (s), 1592 (s), 1543 (s), 1494 (s), 1456 (s), 1404 (s), 1334 (s), 1314 (s), 1302(s), 1273 (s), 1246 (s), 1195 (s), 1175 (s), 1141(s), 1109(s), 1094(s), 1045(s), 1007(m), 931(s), 883(s), 851(s), 802(s), 750(s), 704(s), 645(s), 587(s), 566(s). ^1H NMR (600 MHz, DMSO-d_6 , ppm): 9.58(s, N-H), 9.12(s, N-H), 8.19 (d, $J = 9$ Hz, 2H), 7.70 (d, $J = 9$ Hz, 2H), 7.58 (d, $J = 8$ Hz, 2H), 7.42 (d, $J = 9$ Hz, 2H), 5.78 (s, 1H), 3.16 (t, $J = 8$ Hz, 8H), 1.59- 1.54 (m, 8H), 1.34- 1.27 (m, 8H), 0.93(t, $J = 7$ Hz, 12H). Same reaction with excess amounts of TBABr (5 mmol) instead of TBAF yielded the same salt.

Synthesis of butyl-SMZU.TBAI: A solution of refluxed tetrabutylammonium iodide (185 mg, 0.5 mmol) and **HSMZU** (42 mg, 0.1 mmol) in DMF (10 ml) was stirred at 80°C for 6 hs and the

resulting solution left undisturbed for 8 days yielded crystals of the salt. The supernatant liquid was decanted and the crystals were dried by pressing filter paper (yield 49 %). IR (Neat, cm^{-1}): 2958 (s), 2934 (w), 2873(m), 1713 (s), 1611 (m), 1590 (s), 1560 (s), 1539 (s), 1508(s), 1493 (s), 1448 (s), 1405(m), 1374(m), 1341 (s), 1314 (m), 1304 (s), 1247 (s), 1198 (s), 1162 (s), 1113 (s), 1092 (s), 1027 (s), 925 (w), 882 (s), 856 (s), 827 (m), 804 (m), 749 (s), 712 (s), 678 (s), 645 (s), 594 (s), 569 (s), 556 (s). ^1H NMR (600 MHz, DMSO-d_6 , ppm): 9.59 (s, N-H), 9.45 (s, N-H), 8.21 (d, $J = 9$ Hz, 2H), 7.77 (d, $J = 8$ Hz, 2H), 7.70 (d, $J = 10$ Hz, 2H), 7.68 (d, $J = 9$ Hz, 2H), 6.44 (s, 1H), 3.69 (t, $J = 7$ Hz, 3H), 3.18-3.15 (t, $J = 8$ Hz, 8H), 2.37 (s, 3H), 1.59-1.54 (m, 10H), 1.34-1.28 (m, 10H), 0.94(t, $J = 7$ Hz, 12H), 0.87 (t, $J = 7$ Hz, 3H). ^{13}C NMR (125 MHz, DMSO-d_6): 170.8, 159.2, 151.7, 145.8, 144.1, 141.4, 130.4, 128.4, 125.2, 118.3, 117.9, 97.8, 57.5, 48.1, 29.8, 23.1, 19.2, 13.5, 12.2.

HSTZU.DMF: A solution of 4-nitrophenylisocyanate (328 mg, 2 mmol) (20 ml), sulfathiazole (511 mg, 2 mmol) in dry acetonitrile (20 ml) was stirred for 8 h. This yielded yellow precipitate, which was filtered. It was dissolved in DMF (3 ml) and kept undisturbed condition for crystallization. Needle shaped crystals of HSTZU.DMF were formed after 2-3 days (yield, 81 %). IR (Neat cm^{-1}) : 3093 (bs), 1725 (s), 1651 (s), 1588 (s), 1567 (s), 1526 (s), 1492 (s), 1414 (s), 1331 (s), 1301 (s), 1249 (s), 1190 (s), 1173 (s), 1145 (s), 1102 (s), 1087 (s), 927 (s), 851 (s), 828 (s), 733 (s), 711 (s), 690 (s), 669 (s), 649 (s), 631 (s), 602 (s), 575 (s), 559 (s). ^1H NMR (600 MHz, DMSO-d_6 , ppm): 12.70 (s, 1H), 9.53 (s, N-H), 9.31 (s, N-H), 8.21 (d, $J = 9$ Hz, 2H), 7.94 (s, 1H), 7.74 (d, $J = \text{Hz}$, 2H), 7.70 (d, $J = 9$ Hz, 2H), 7.61 (d, $J = 9$ Hz, 2H), 7.24 (d, $J = 5$ Hz, 1H), 6.82 (d, $J = 4$ Hz, 1H), 2.88 (s, 3H), 2.72 (s, 3H). ^{13}C NMR (125 MHz, DMSO-d_6): 168.8, 162.5, 151.9, 146.1, 142.5, 141.4, 135.6, 127.2, 125.3, 118.1, 117.9, 108.2, 35.9, 30.9.

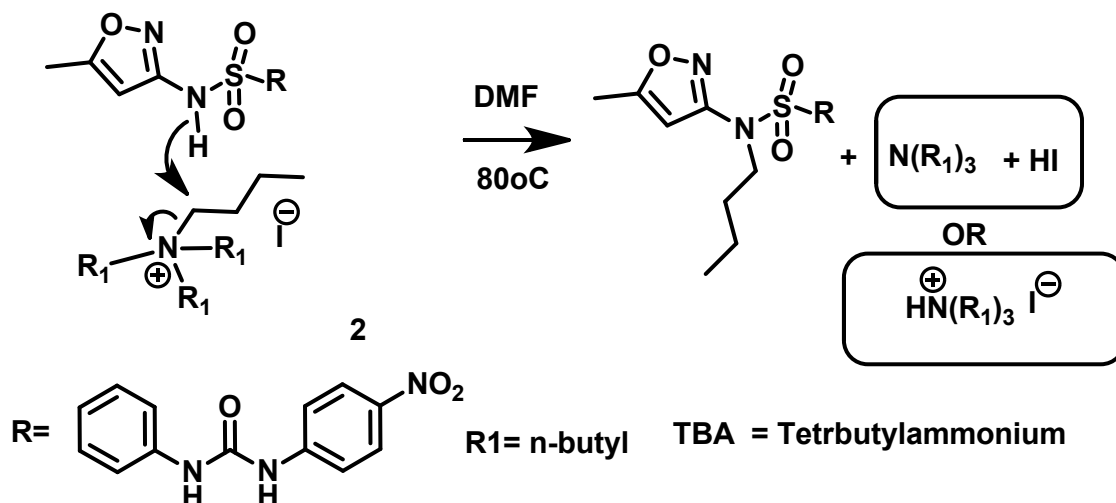
HSTZU.DMSO: The HSTZU (42 mg, 0.1 mmol) was dissolved in DMSO (0.5 ml) in a plastic vial (1ml capacity) and left undisturbed for crystallization. Block type of crystals of HSTZU.DMSO were formed in a week. The crystals were collected by decanting the supernatant liquid. IR (Neat, cm^{-1}) : 3101 (bs), 1716 (s), 1595 (s), 1538 (s), 1489 (s), 1435 (s), 1332 (s), 1299 (s), 1246 (s), 1195 (s), 1174 (s), 1143 (s), 1113 (s), 1088 (s), 1011 (s), 939 (s), 849 (s), 733 (s), 709 (s), 652 (s), 631 (s), 576 (s), 552 (s). ^1H NMR (600 MHz, DMSO-d_6 , ppm): 12.67 (s, 1H), 9.51(s, N-H), 9.29 (s, N-H), 8.21 (d, $J = 9$ Hz, 2H), 7.74 (d, $J = 8$ Hz, 2H), 7.70 (d, $J = 9$ Hz, 2H), 7.60 (d, $J = 9$ Hz), 7.24 (d, $J = 4$ Hz, 1H), 6.82 (d, $J = 4$ Hz, 1H), 2.54 (s, 6H

) . ^{13}C NMR (125 MHz, DMSO-d_6): 168.7, 151.8, 145.9, 142.4, 141.3, 135.6, 127.1, 125.2, 124.4, 118.0, 117.8, 108.1.

HSTZU.TBAI: Cocrystal of HSTZU with tetrabutylammonium iodide was prepared by stirring a mixture of HSTZU (42 mg, 0.1 mmol) with ten equivalents amounts of TBAI (369 mg, 1 mmol) in DMF (10ml) for 5 mins at room temperature. The mixture was filtered and filtrate was kept in open air for slow evaporation to obtain the crystals of HSTZU.TBAI after 12 days (yield 53 %). IR (Neat, cm^{-1}): 2958 (m), 2870 (m), 1713 (s), 1590 (s), 1560 (s), 1536 (s), 1493 (s), 1411 (s), 1302 (s), 1245 (s), 1196 (s), 1146 (s), 1112 (s), 1087 (s), 934 (s), 854 (s), 740 (s), 702 (s), 650 (s), 634 (s), 574 (s), 558 (s). ^1H NMR (600 MHz, DMSO-d_6 , ppm): 12.67 (s, 1H), 9.52 (s, N-H), 9.29 (s, N-H), 8.20 (d, $J = 9$ Hz, 2H), 7.73 (d, $J = 8$ Hz, 2H), 7.69 (d, $J = 9$ Hz, 2H), 7.60 (d, $J = 8$ Hz, 2H), 7.24 (d, $J = 5$ Hz, 1H), 6.81 (d, $J = 4$ Hz, 1H), 3.15 (t, 8H), 1.59- 1.54 (m, 8H), 1.34- 1.28 (m, 8H), 0.93 (t, 12H). ^{13}C NMR (125 MHz, DMSO-d_6): 168.7, 151.8, 145.9, 142.4, 141.3, 135.6, 127.1, 125.2, 124.4, 117.9, 117.8, 108.1, 57.5, 23.1, 19.2, 13.5.

TBA(STZU) : A solution of tetrabutylammonium fluoride trihydrate (63 mg, 0.2 mmol) HSTZU (42 mg, 0.1 mmol) in DMF (5 ml) was stirred for 1 h to obtain TBA(STZU) as a white precipitate. IR (Neat cm^{-1}) : 2959 (m), 2872 (m), 1709 (s), 1657 (s), 1592 (s), 1539 (s), 1495 (s), 1433 (s), 1304 (s), 1266 (m), 1233 (s), 1201 (s), 1178 (s), 1164 (m), 1141 (s), 1091 (s), 948 (s), 856 (s), 842 (s), 752 (s), 736 (s), 697 (s), 655 (s), 644 (s), 618 (s), 576 (s), 560 (s). ^1H NMR (600 MHz, DMSO-d_6 , ppm): 9.61 (s, N-H), 9.17 (s, N-H), 8.18 (d, $J = 9$ Hz, 2H), 7.69 (d, $J = 9$ Hz, 2H), 7.63 (d, $J = 8$ Hz, 2H), 7.42 (d, $J = 9$ Hz, 2H), 6.920 (d, $J = 4$ Hz, 1H), 6.43 (d, $J = 4$ Hz, 1H), 3.16 (t, 8H), 1.59- 1.54 (m, 8H), 1.33- 1.27 (m, 8H), 0.93 (t, 12H). ^{13}C NMR (125 MHz, DMSO-d_6): 169.6, 151.8, 146.3, 141.1, 140.4, 139.7, 136.9, 126.9, 125.1, 117.6, 117.4, 107.1, 57.5, 23.1, 19.2, 13.5.

All the solvates and cocrystals were stable at room temperature under ambient conditions at least for a week.



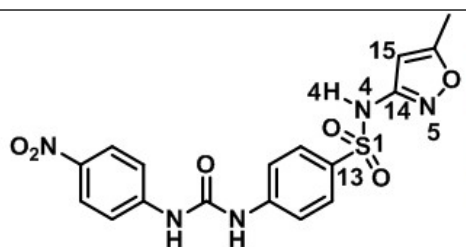
Scheme S1: A plausible mechanism of the C-N bond formation from reaction of HSTZU with TBAI

Table S1: Hydrogen bond parameters of solvates, cocrystals and salt.

Solvate/salt/cocrystal	D-H...A (Symmetry)	$d_{\text{D-H}}$ (Å)	$d_{\text{H...A}}$ (Å)	$d_{\text{D...A}}$ (Å)	$\angle\text{D-H...A}$ (°)
HSMZU.DMF-P1	N(2)-H(2N) ...O(7) [1/2-x, 1/2+y, 1/2-z]	0.80(4)	2.15(4)	2.897(6)	155(4)
	N(3)-H(3N) ...O(7) [1/2-x, 1/2+y, 1/2-z]	0.77(4)	2.12(4)	2.839(6)	156(4)
	N(4)-H(4N) ...O(5) [1+x, y, z]	0.85(4)	2.27(4)	3.091(4)	163(4)
	C(2)-H(2) ...O(3) [2-x, 1-y, -z]	0.93	2.56(5)	3.455(5)	161
	C(9)-H(9) ...O(1) [2-x, 1-y, -z]	0.93	2.53	3.234(5)	133
	C(15)-H(15) ...N(5) [-1+x, y, z]	0.93	2.30	3.198(5)	161
	C(19)-H(19C) ...O(2) [-x, 1-y, -z]	0.96	2.37	3.151(19)	138
HSMZU.DMF-P2	N(2)-H(2N) ...O(5) [-x, 1-y, -z]	0.86	2.21	2.975(3)	148
	N(3)-H(3N) ...N(5) [-x, 1-y, -z]	0.86	2.19	3.050(3)	174
	N(4)-H(4N) ...O(7) [-1+x, 1+y, z]	0.86	1.99	2.704(3)	139
	C(2)-H(2A) ...O(3) [1-x, 1-y, 1-z]	0.93	2.57	3.424(3)	152
	C(15)-H(15) ...O(2) [-1+x, 1+y, z]	0.93	2.54	3.331(4)	142
TBA(SMZU)	N(2)-H(2N) ...N(4) [1+x, y, z]	0.86	2.28	3.081(3)	162
	N(3)-H(3N) ...N(4) [1+x, y, z]	0.86	2.09	2.928(3)	159
	C(9)-H(9) ...O(1) [2-x, 1-y, 1-z]	0.93	2.50	3.192(3)	172
	C(17)-H(17B) ...O(5) [1-x, 1-y, -z]	0.96	2.42	3.322(4)	153
	C(22)-H(22A) ...O(4) [x, y, z]	0.97	2.39	3.340(3)	166

butyl-SMZU.TBAI	N(2) -H(2N) ...I1 [-1+x, y, z]	0.86	2.77	3.594(4)	163
	N(3) -H(3N) ...I1 [-1+x, y, z]	0.86	2.75	3.569(5)	160
	C(33) -H(33B) ...O(4) [x, 1+y, z]	0.97	2.35	3.294(6)	163
	C(34) -H(34BB) ... O(1) [1-x, 2-y, 1-z]	0.97	2.42	3.326(7)	156
	C(37) -H(37B) ... O(2) [-x, 2-y, 1-z]	0.97	2.49	3.40(3)	156
HSTZU.DMF	N(2) -H(2N) ... O(6) [1+x, y, z]	0.77	2.13	2.843(5)	154
	N(3) -H(3N) ... O(6) [1+x, y, z]	0.77	2.17	2.881(5)	152
	N(5) -H(5N) ... N(4) [-x, 1-y, -z]	0.85	2.04	2.896(5)	177
	C(9) -H(9) ... O(1) [1-x, 1-y, 1-z]	0.93	2.55	3.187(6)	126
	C(18) -H(18C) ... S(2) [1/2+x, 1/2-y 1/2+z]	0.96	2.83	3.591(6)	137
HSTZU.DMSO	N(2) -H(2N) ...O(6) [x, 1/2-y, -1/2+z]	1.01(5)	1.94(5)	2.913(8)	160(4)
	N(3) -H(3N) ...O(6) [x, 1/2-y, -1/2+z]	0.90(5)	2.08(5)	2.907(8)	153(4)
	N(5) -H(5N) ...N(4) [-x, 1-y, -z]	0.97(5)	1.88(5)	2.838(9)	173(4)
	C(2) -H(2) ...O(1) [1-x, 1/2+y, 1/2-z]	0.93	2.52	3.216(11)	132
	C(3) -H(3) ...O(2) [1-x, -2-y, -z]	0.93	2.42	3.328(11)	166
	C(17) -H(17B) ...O(3) [x, y, z]	0.96	2.46	3.335(10)	152
HSTZU.TBAI	N(2) -H(2N) ...I(1) [1+x, y, z]	0.79(6)	2.93(6)	3.669(6)	159(6)
	N(3) -H(3N) ...I(1) [1+x, y, z]	0.71(5)	2.83(5)	3.511(7)	160(5)
	N(5) -H(5N) ...N(4) [1-x, 1-y, -z]	0.83(7)	2.04(7)	2.854(8)	166(5)
	C(20) -H(20B) ...O(2) [1-x, -y, 1-z]	0.97	2.50	3.436(8)	162
	C(21) -H(21B) ...O(5) [x, -1+y, z]	0.97	2.30	3.253(8)	168

Table S2: Torsion angles of solvates, ionic cocrystals and salts of HSMZU

	Torsion angle(°)	HSMZU.DMF-P2	HSMZU.DMF-P1
	C13-S1-N4-C14	57.6(2)	60.6(4)
	C13-S1-N4-H4N	-122.4	-86(3)
	H4N-N4-C14-C15	23.6	179(3)
	H4N-N4-C14-N5	-154.8	-2(3)

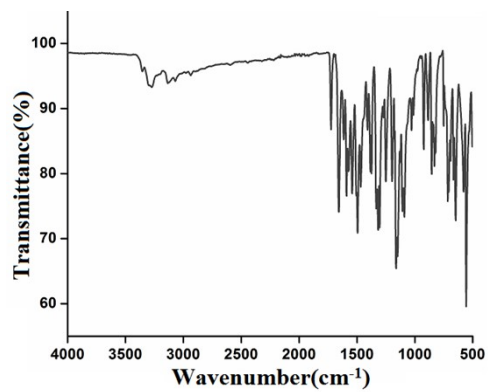


Figure S3: FT-IR spectrum (neat) of the **HSMZU.DMF-P1**.

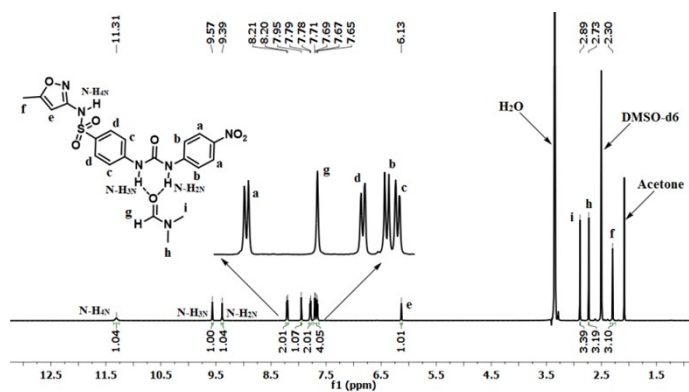


Figure S4: ^1H NMR (DMSO- d_6 , 600 MHz) spectra of the **HSMZU.DMF-P1**.

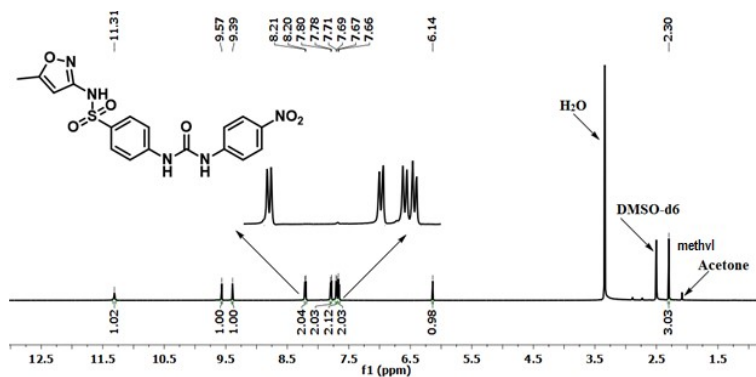


Figure S5: ^1H NMR (DMSO- d_6 , 600 MHz) spectra of the **HSMZU**.

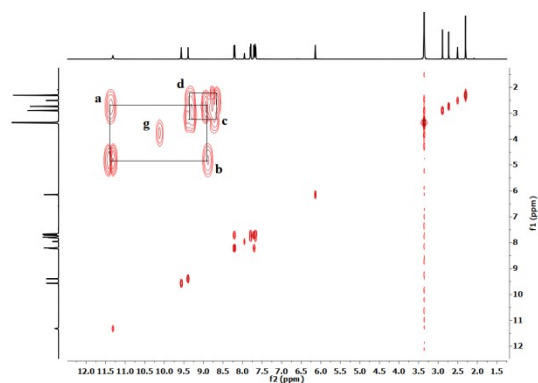


Figure S6: ^1H -2D-HOMOCOSY (600 MHz, DMSO-d_6) spectrum of the **HSMZU.DMF-P1**.

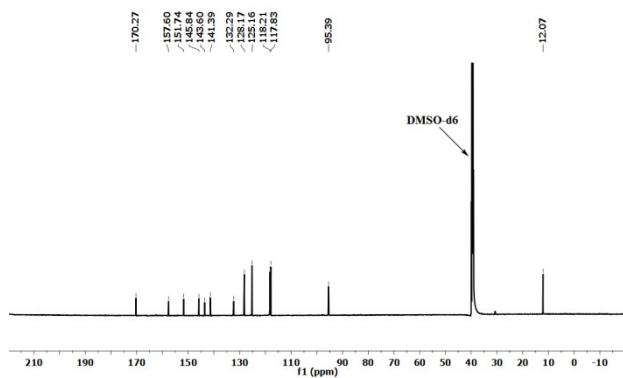


Figure S7: ^{13}C NMR (125 MHz, DMSO-d_6) spectrum of the **HSMZU.DMF-P1**.

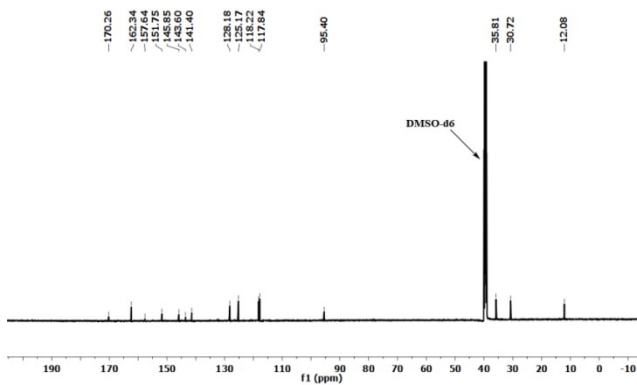


Figure S8: ^{13}C NMR (125 MHz, DMSO-d_6) spectra of the **HSMZU.DMF-P1**.

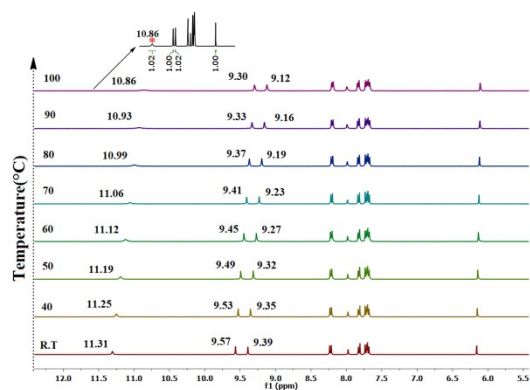


Figure S9: ^1H NMR (DMSO- d_6 , 600 MHz) spectra of the **HSMZU.DMF-P1** at variable temperatures.

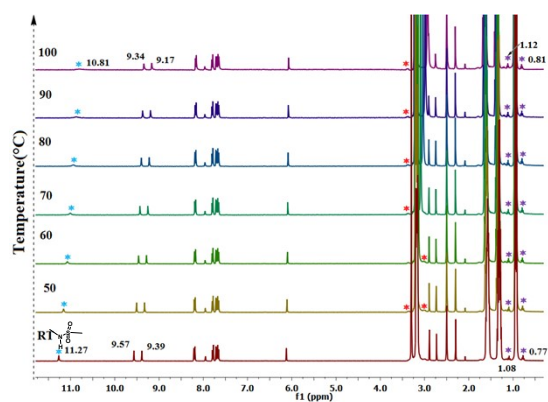
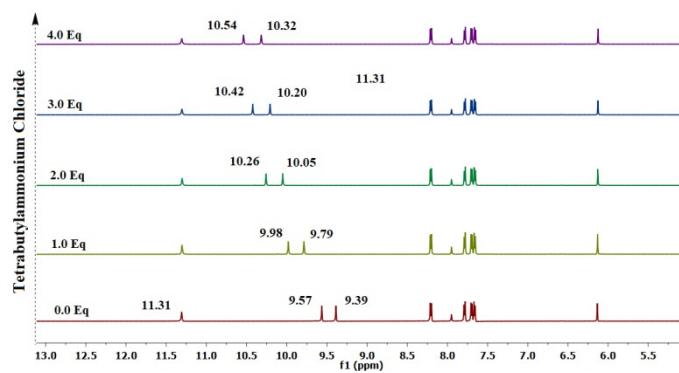
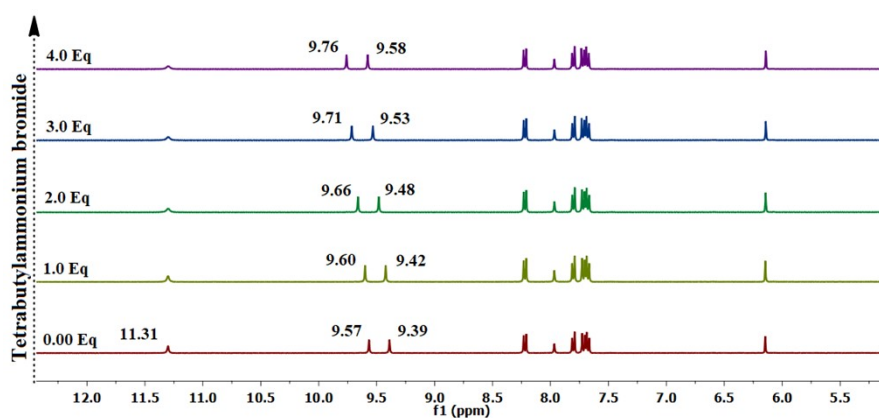


Figure S10: Variable temperature ^1H NMR spectra (DMSO- d_6 , 600 MHz) of **HSMZU.DMF-P1** with 10 equivalent of **TBAI** showing C-N bond formation to form the butyl-**SMZU.TBAI** (In situ in the reaction mixture. {As per the Scheme S1 there are three types of butyl environments from the three compounds in the reaction mixture which are $\text{N}^+(\text{CH}_2^a\text{CH}_2^b\text{CH}_2^c\text{CH}_3^d)_4\text{I}$, $(\text{CH}_2^{a'}\text{CH}_2^{b'}\text{CH}_2^{c'}\text{CH}_3^{d'})\text{-SMZU}$ and $\text{N}(\text{CH}_2^{a''}\text{CH}_2^{b''}\text{CH}_2^{c''}\text{CH}_3^{d''})_3$. The protons from the $\text{CH}_2^b\text{CH}_2^c$, $\text{CH}_2^{b'}\text{CH}_2^{c'}$, $\text{CH}_2^{b''}\text{CH}_2^{c''}$ are indistinguishable as they overlap each other; the peaks with * (red asterisk) are from $\text{CH}_2^{a'}$ and $\text{CH}_2^{a''}$ and with * (violet asterisk) are from $\text{CH}_3^{d'}$ and $\text{CH}_3^{d''}$ respectively. The peak at 11.17 marked with * (blue asterisk) is from the N-H next to the heterocycle).



(a)



(b)

Figure S11: ^1H NMR (600 MHz, DMSO-d_6) titration of **HSMZU.DMF-P1** by adding different amounts of tetrabutylammonium (a) chloride and (b) bromide (showing the aromatic protons of **HSMZU.DMF-P1**).

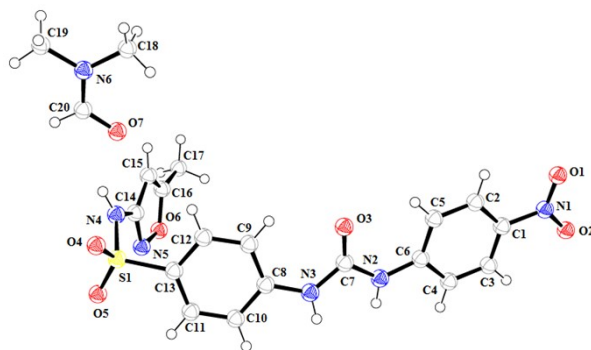


Figure S12: ORTEP diagram of **HSMZU.DMF-P2** drawn with 50% ellipsoid probability.

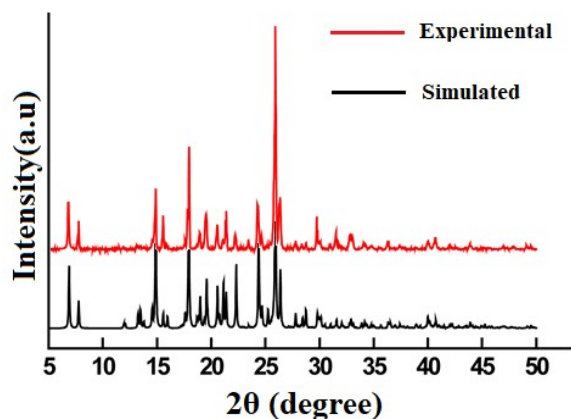


Figure S13 : Powder X-ray diffraction patterns of the **HSMZU.DMF-P2**.

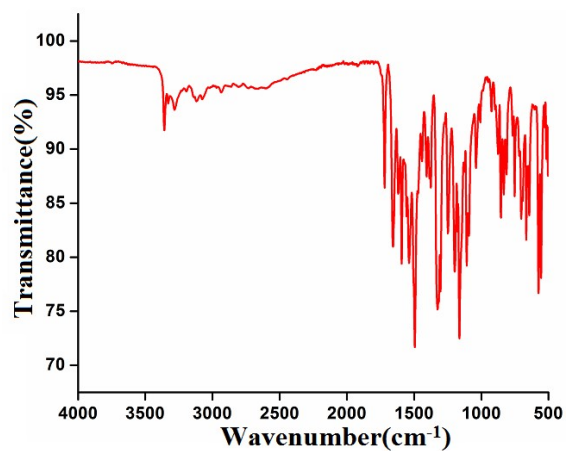


Figure S14: FT-IR spectrum (neat) of the **HSM** Figure S13: Powder X-ray diffraction patterns of the **HSMZU.DMF-P2**.

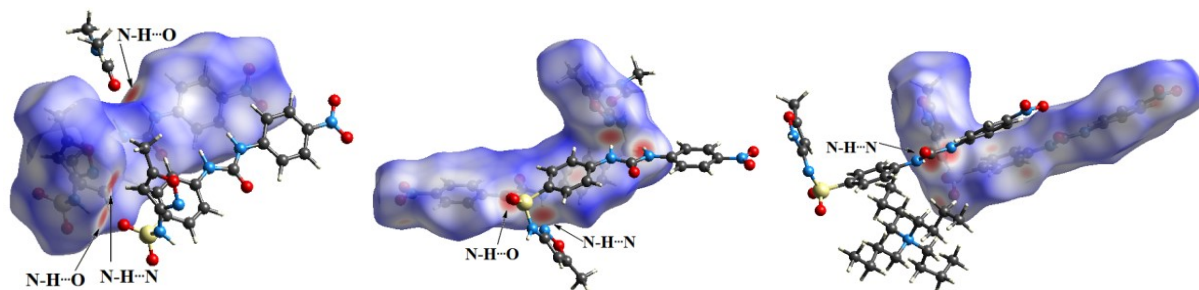


Figure S15 : Hirshfeld surfaces of (d) **HSMZU.DMF-P1**, (e) **HSMZU.DMF-P2**, (f) **TBA(SMZU)**

Figure S18: FT-IR spectrum (neat) of the TBA(SMZU).

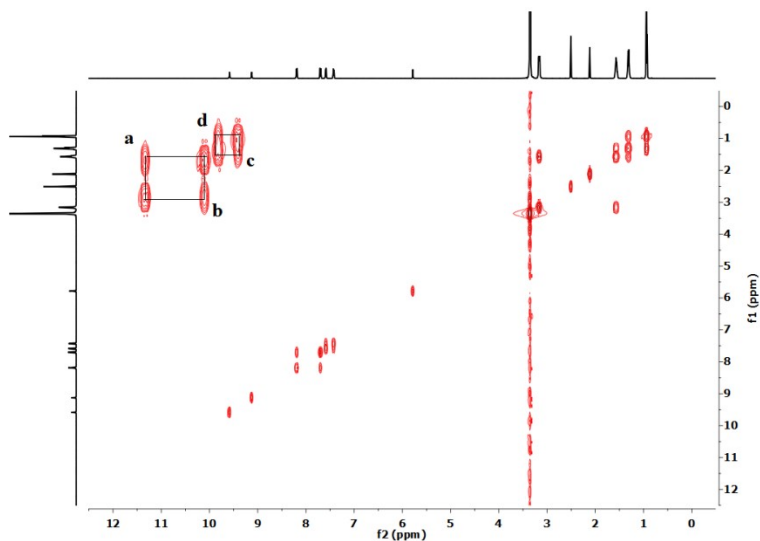


Figure S19: ¹H 2D-HOMOCOSY (600 MHz, DMSO-d₆) spectrum of the TBA(SMZU).

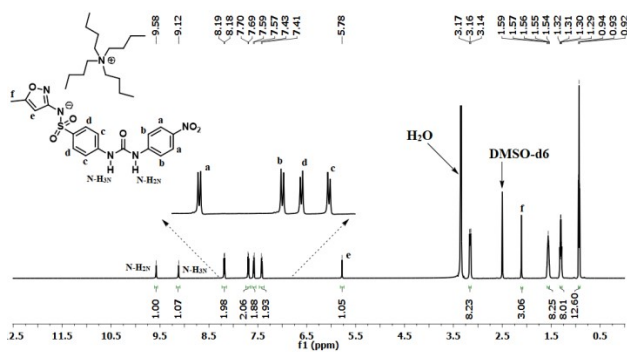


Figure S20: ¹HNMR (DMSO-d₆, 600 MHz) spectra of the TBA(SMZU). Figure S18: ¹H 2D-HOMOCOSY (600 MHz, DMSO-d₆) spectrum of the TBA(SMZU).

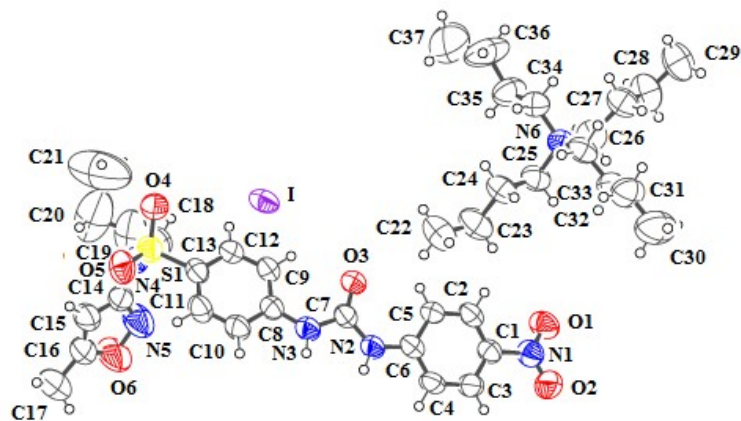


Figure S21: ORTEP diagram of butyl-SMZU.TBAI drawn with 50% ellipsoid probability.

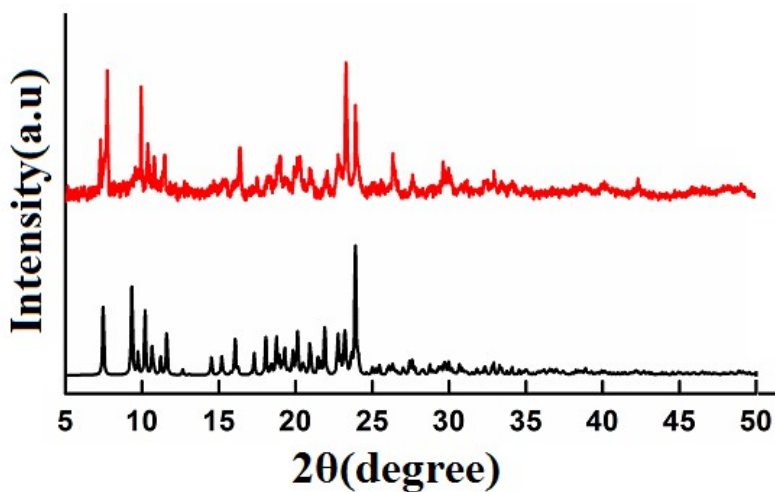


Figure S22: Powder X-ray diffraction patterns of the butyl-SMZU.TBAI

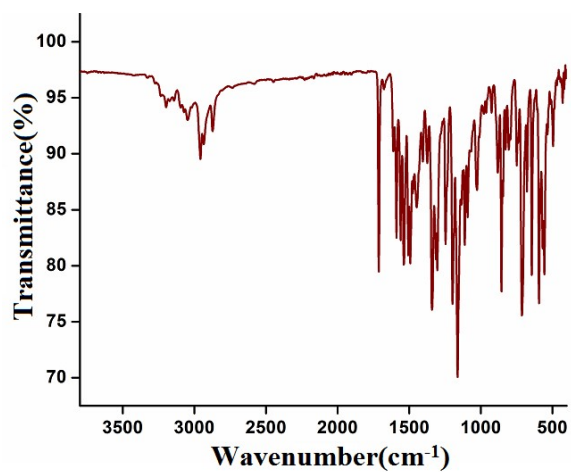


Figure S23: FT-IR spectrum (neat) of the butyl-SMZU.TBAI.

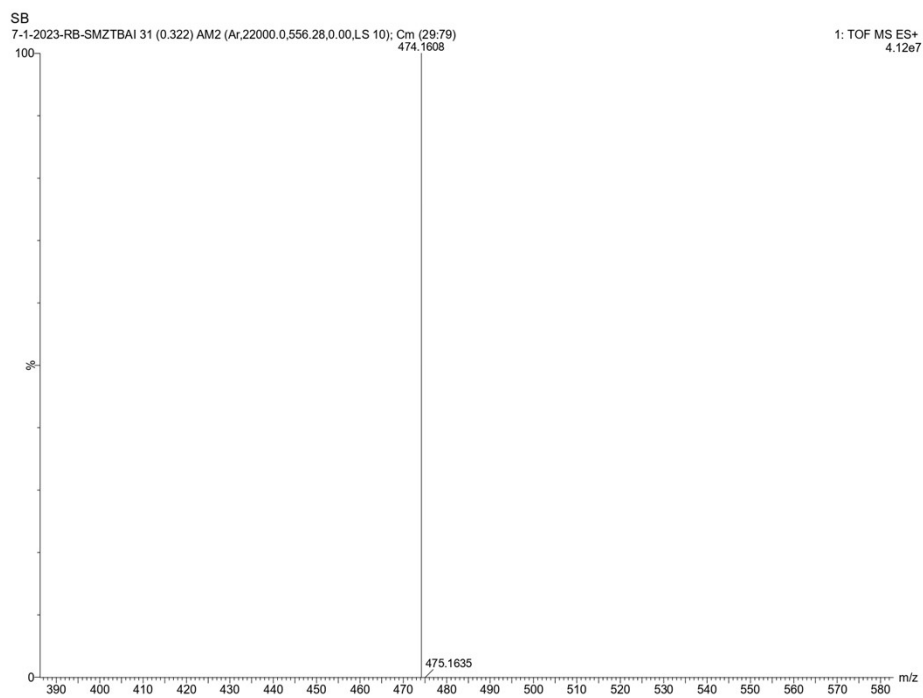


Figure S26: ESI mass spectrum of the butyl-SMZU.

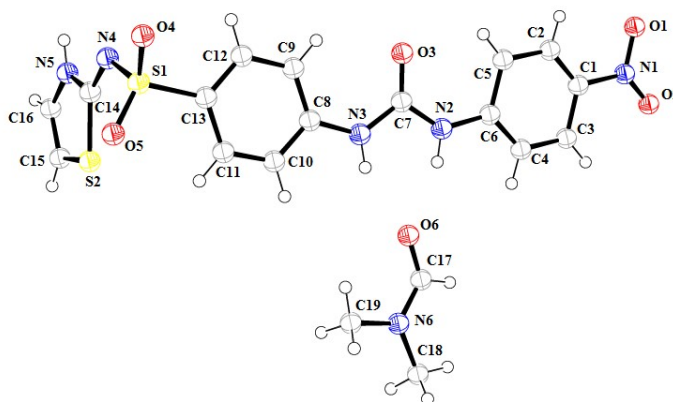


Figure S27: ORTEP diagram of HSTZU.DMF drawn with 50% ellipsoid probability.

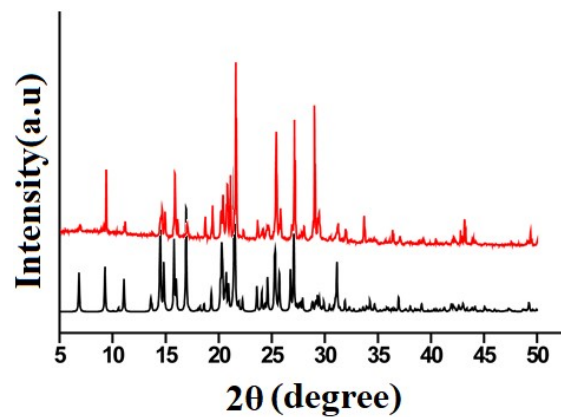


Figure S28: Powder X-ray diffraction patterns of the HSTZU.DMF.

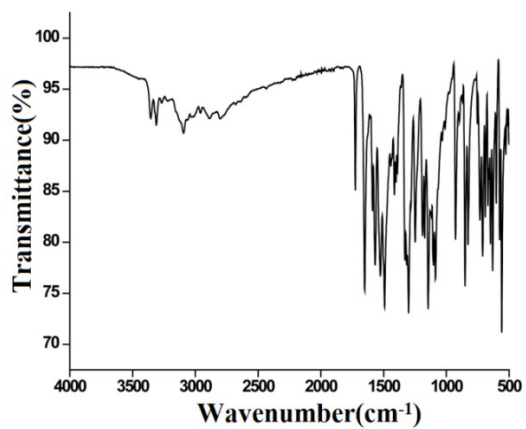


Figure S29: FT-IR spectrum (neat) of the HSTZU.DMF.

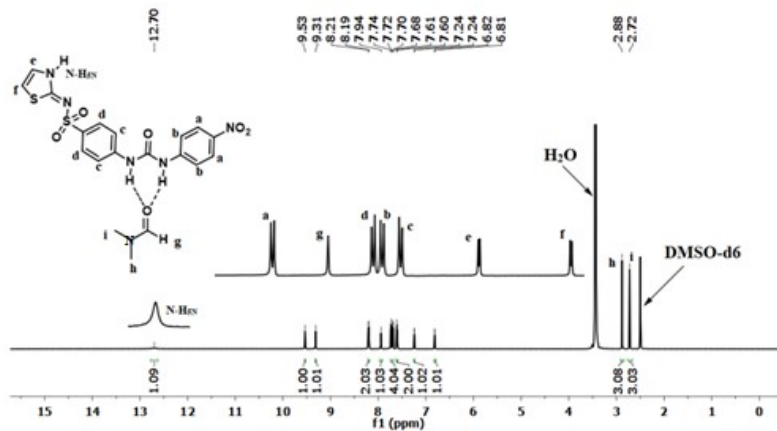


Figure S30: ^1H NMR (DMSO- d_6 , 600 MHz,) spectra of the HSTZ.DMF.

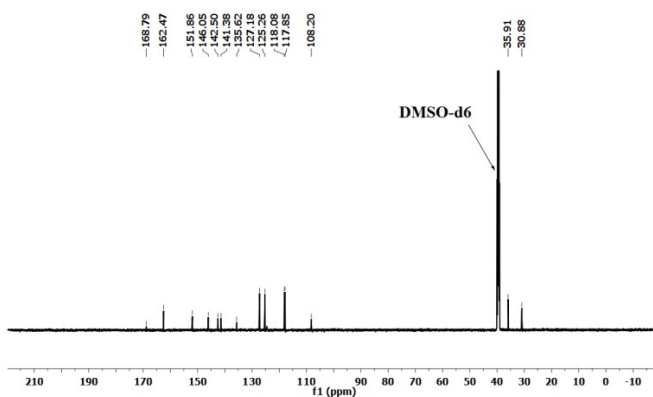
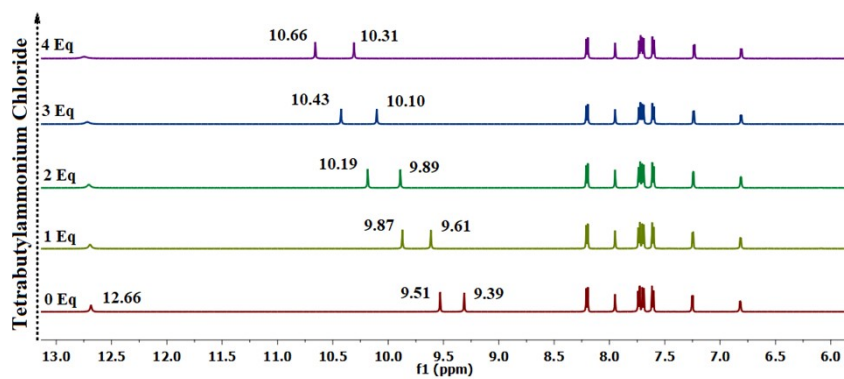
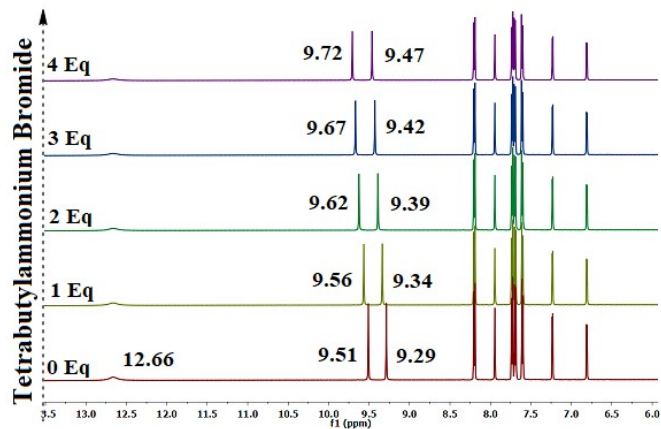


Figure S31: ^{13}C NMR (125 MHz, DMSO- d_6) spectra of the HSTZ.DMF.



(a)



(b)

Figure S32: ^1H NMR (600 MHz, DMSO-d_6) titration showing the aromatic protons of HSTZU.DMF recorded by adding different amounts of tetrabutylammonium (a) chloride and (b) bromide.

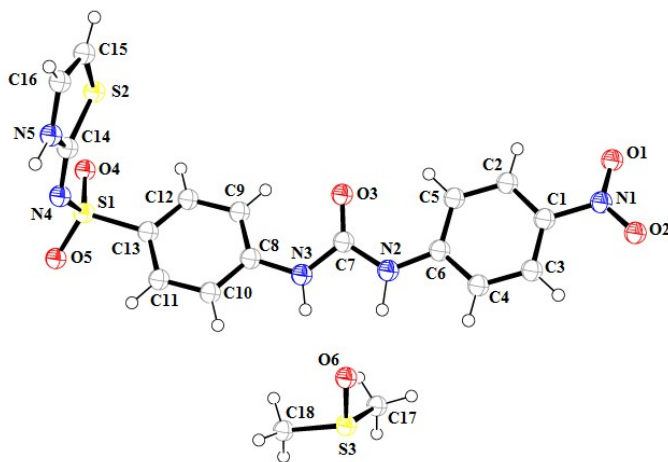


Figure S33: ORTEP diagram of HSTZU.DMSO drawn with 50% ellipsoid probability.

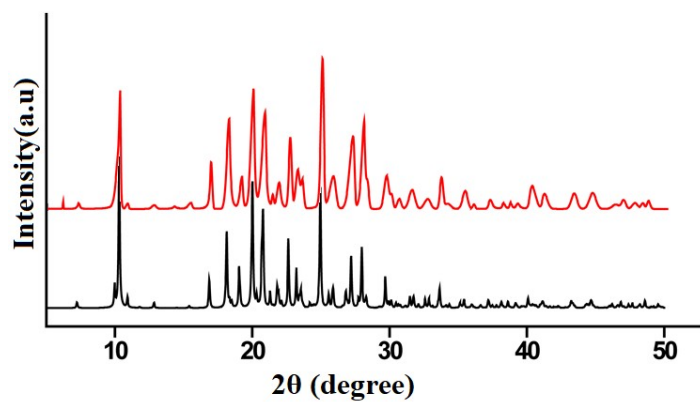


Figure S34: Powder X-ray diffraction patterns of the HSTZU.DMSO.

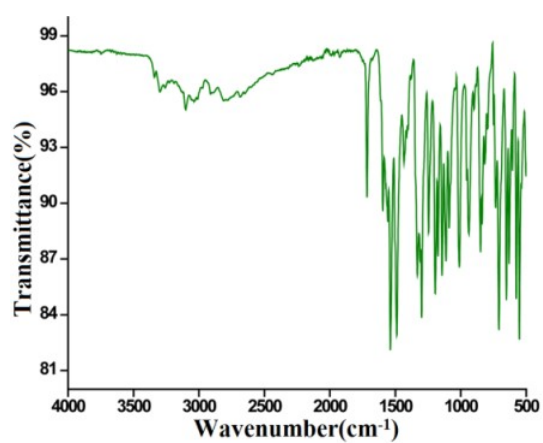


Figure S35: FT-IR spectrum (neat) of the HSTZU.DMSO.

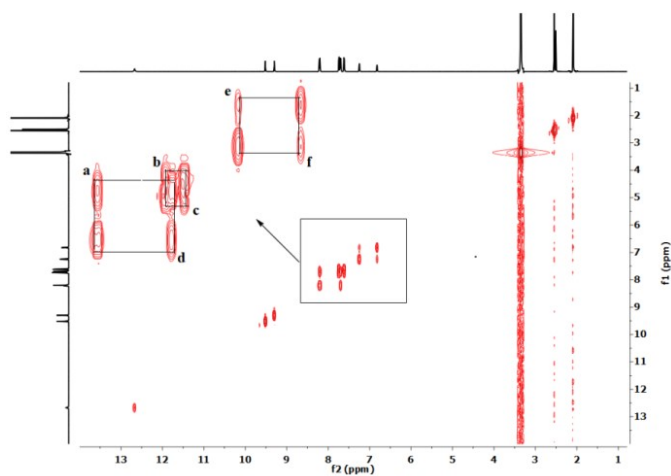


Figure S36: ^1H 2D-HOMOCOSY (600 MHz, DMSO-d_6) spectrum of the HSTZU.DMSO.

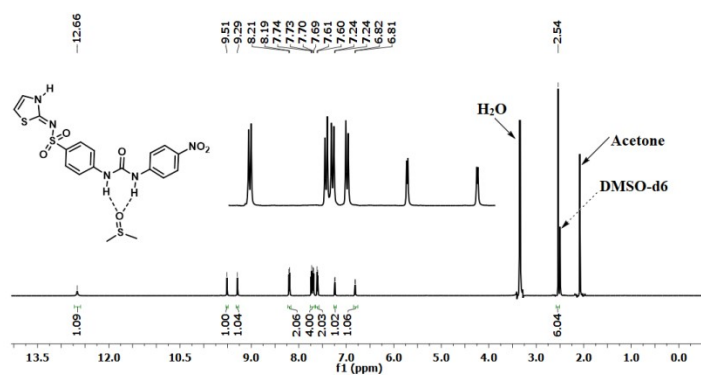


Figure S37: ^1H NMR (DMSO- d_6 , 600 MHz,) spectra of the HSTZU.DMSO.

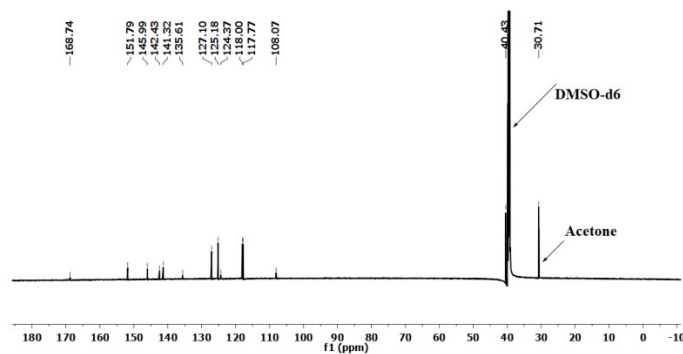


Figure S38: ^{13}C NMR (125 MHz, DMSO- d_6) spectra of the HSTZU.DMSO.

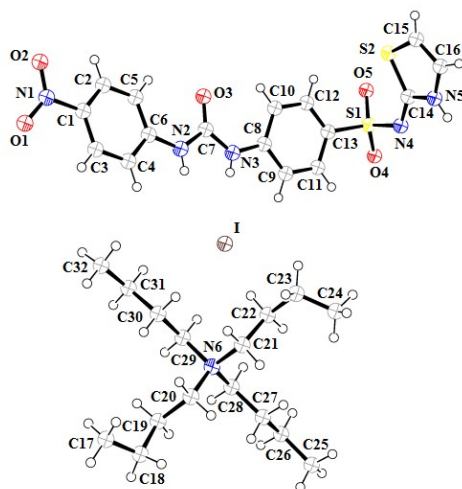


Figure S39: ORTEP diagram of HSTZU.TBAI with 50 % ellipsoid probability.

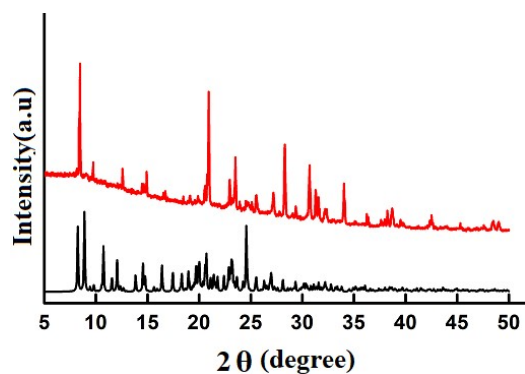


Figure S40: Powder X-ray diffraction patterns of the HSTZU.TBAI.

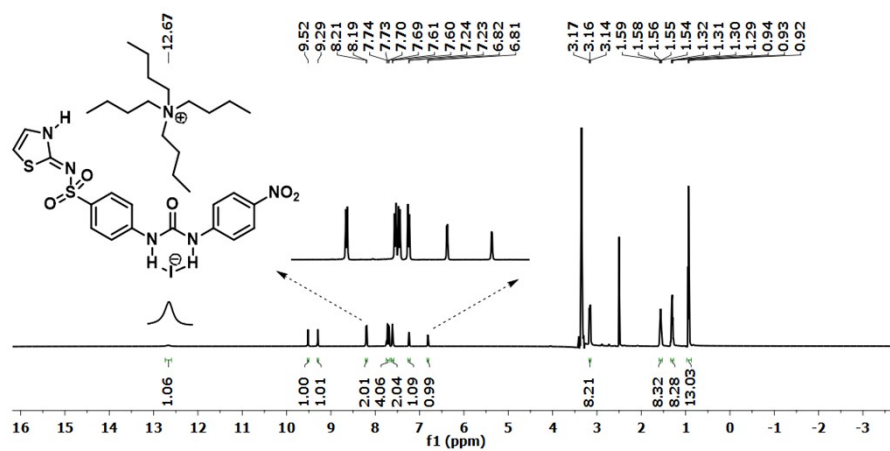


Figure S41: ^1H NMR (DMSO- d_6 , 600 MHz) spectra of the HSTZU.TBAI.

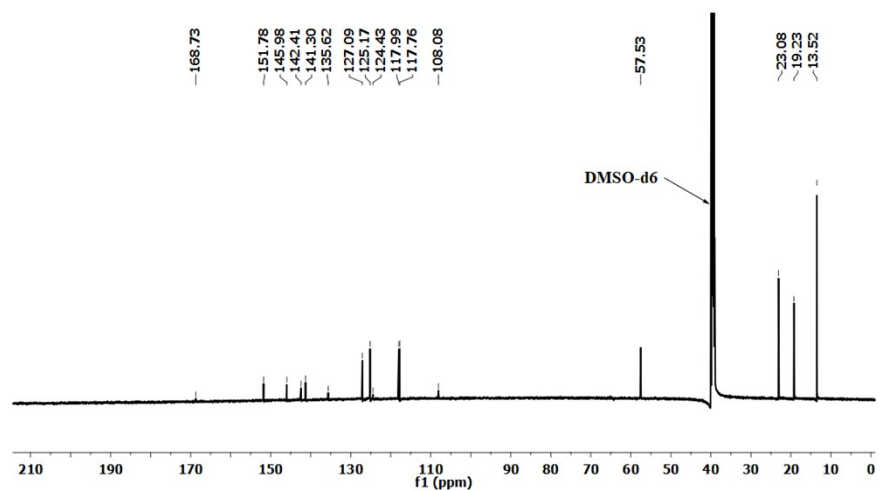


Figure S42: ^{13}C NMR (125 MHz, DMSO-d_6) spectra of the HSTZU.TBAI.

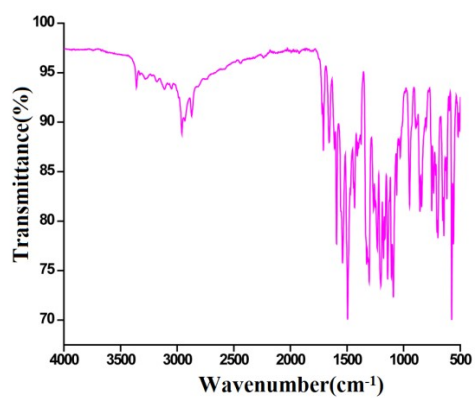


Figure S43: FT-IR spectrum (neat) of the TBA(STZU).

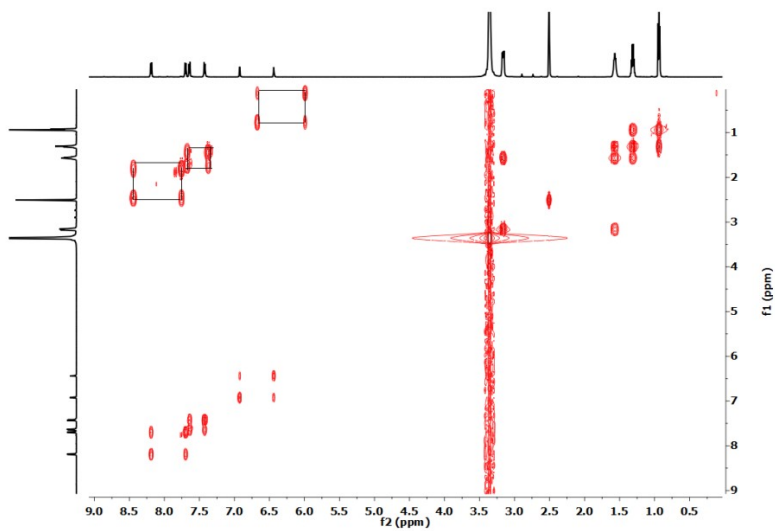


Figure S44: ^1H 2D-HOMOCOSY (600 MHz, DMSO-d_6) spectrum of the TBA(STZU).

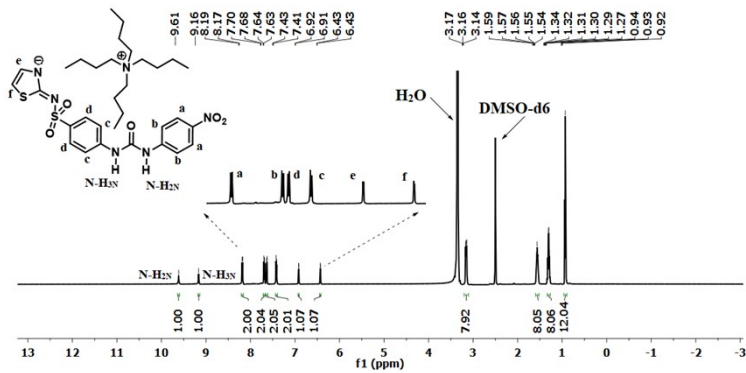


Figure S45: ^1H NMR (DMSO-d_6 , 600 MHz) spectra of the TBA(STZU).

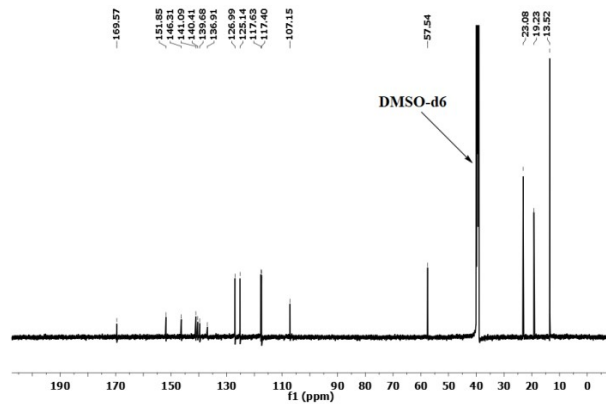
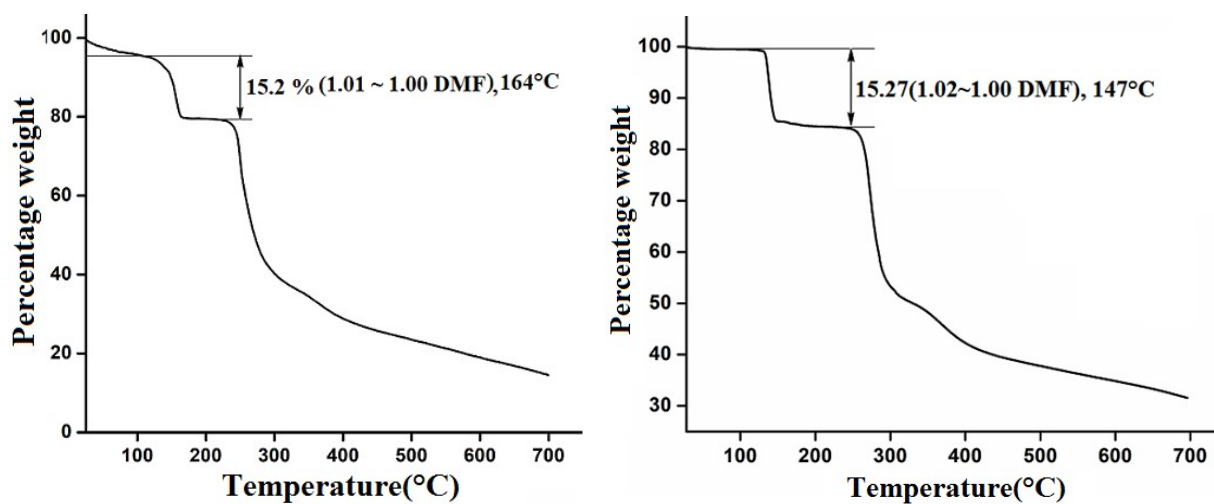


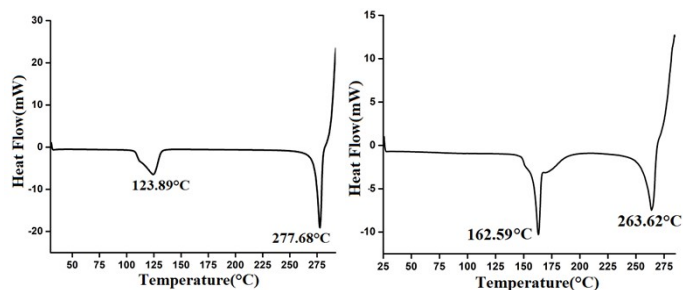
Figure S46: ^{13}C NMR (125 MHz, DMSO-d_6) spectra of the TBA(STZU).



(a)

(b)

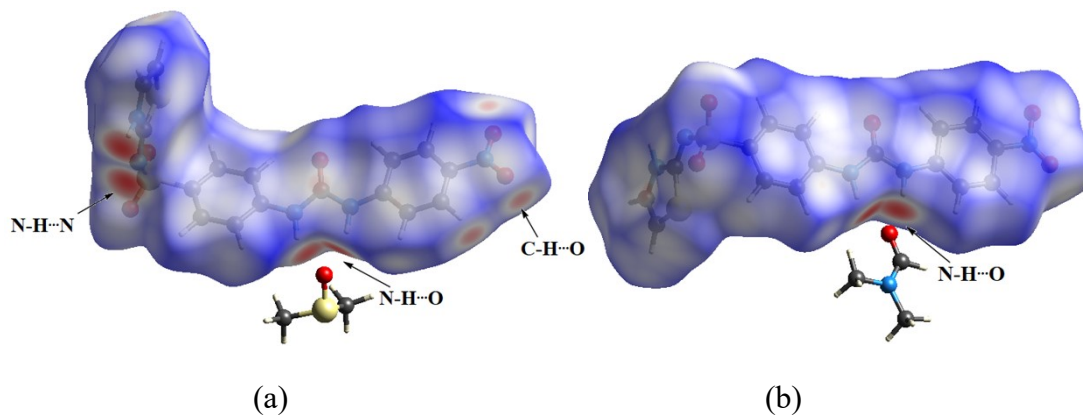
Figure S47: Thermogram of the polymorph (a) HSMZU.DMF-P1 (b) HSMZU.DMF-P2.



(a)

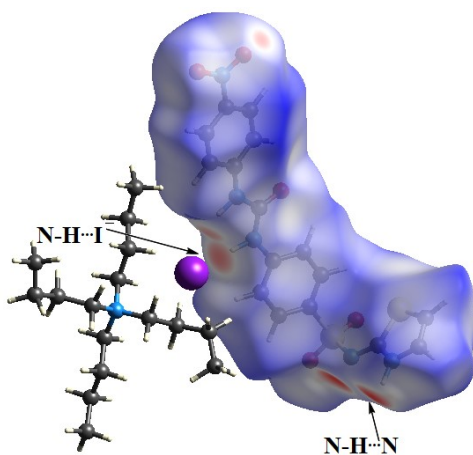
(b)

Figure S48: Differential scanning calorimetry of (a) HSTZU.DMF (b) HSTZU.DMSO (heating rate 10°C/min under nitrogen atmosphere).



(a)

(b)



(c)

Figure S49: Hirshfeld surfaces of (a) HSTZU.DMF (b) HSTZU.DMSO, (c) HSTZU.TBAI.

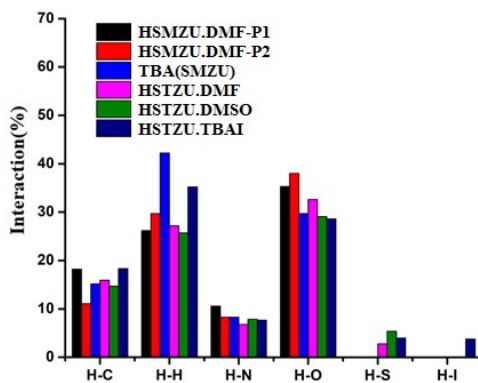


Figure S50: Percentages of the H···C, H···H, H···O, H···N, H···S and H···anion interaction (include reciprocal contacts) in 2D fingerprint plots

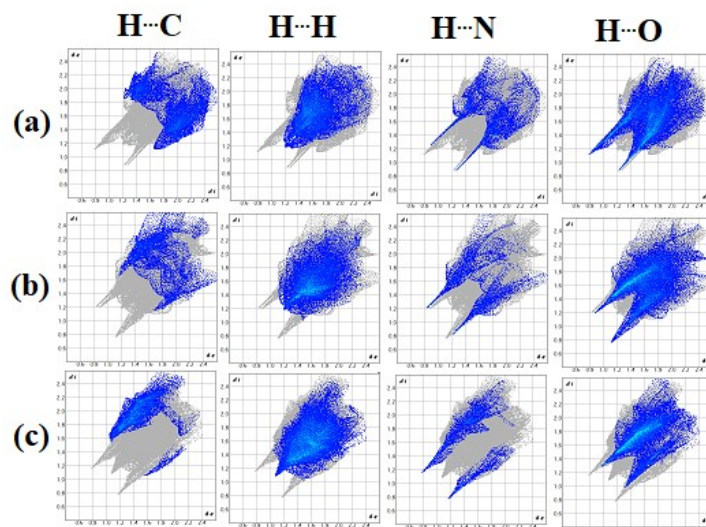


Figure S51: 2D fingerprint plots (including reciprocal contacts) of the H··C, H··H, H··O, H··N and H··anion interactions of a) HSMZU.DMF-P1 b) HSMZU.DMF-P2 c) TBA(SMZU).

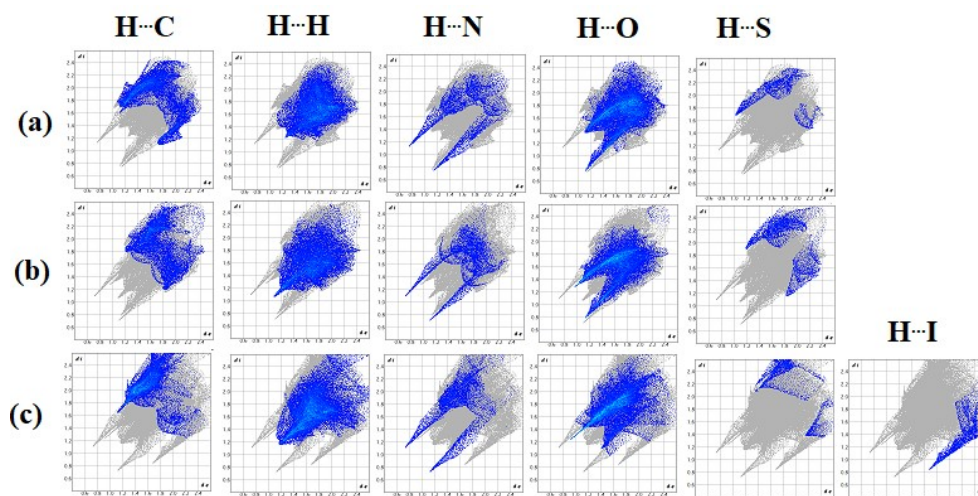


Figure S52: 2D fingerprint plots (including reciprocal contacts) of the H··C, H··H, H··O, H··N and H··anion interactions of (a) HSTZU.DMF (b) HSTZU.DMSO (c) HSTZU.TBAI.

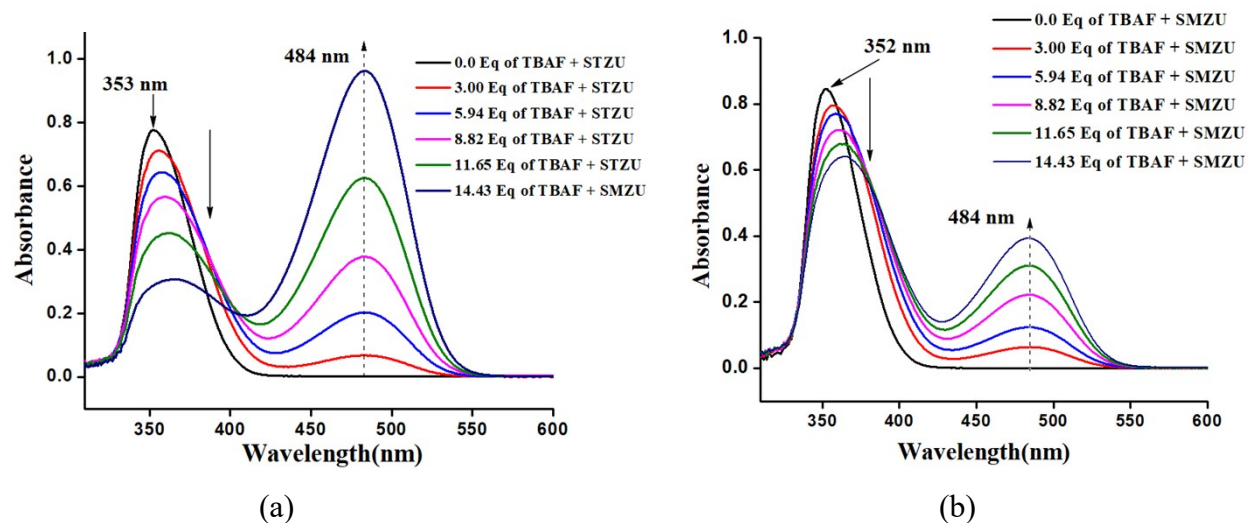


Figure S53: Changes in the UV-visible spectra of (a) HSTZU and (b) HSMZU (3.3×10^{-5} M, 2mL in each case) in dimethylsulfoxide by aliquots (30 μ L) of tetrabutylammonium fluoride (10^{-2} M).

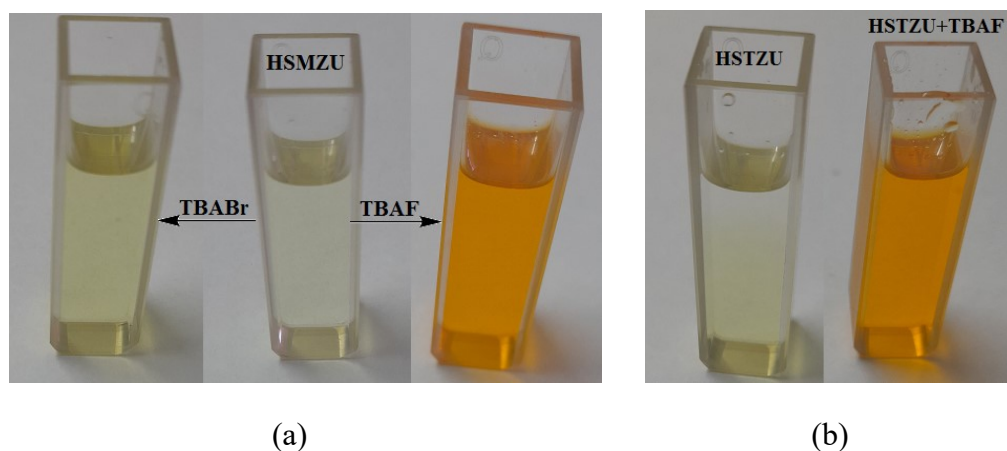
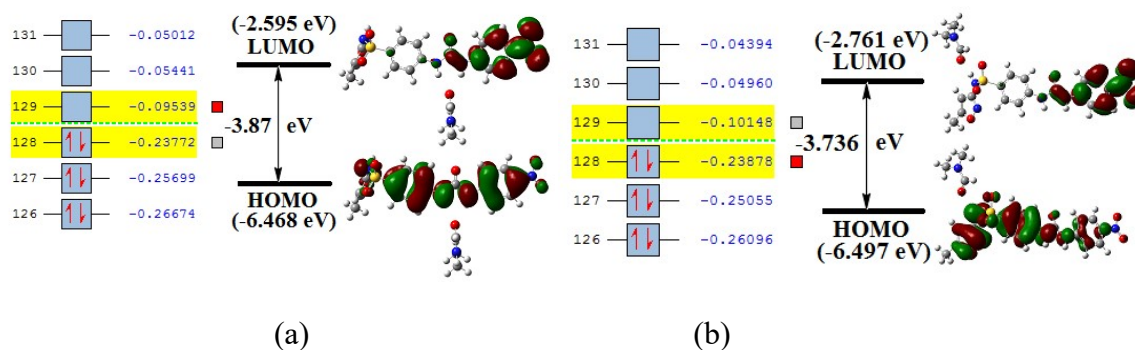
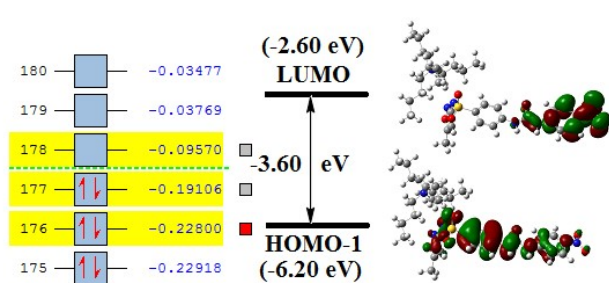
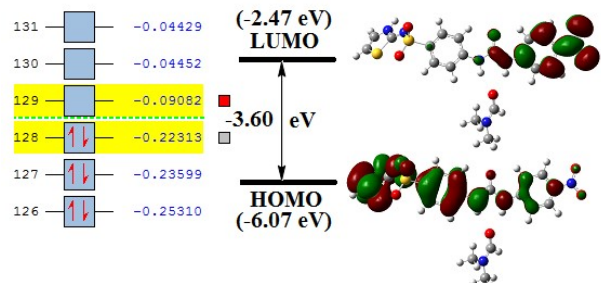


Figure S54: Visual color change of a) HSMZU b) HSTZU after addition of TBAF and TBABr respectively.

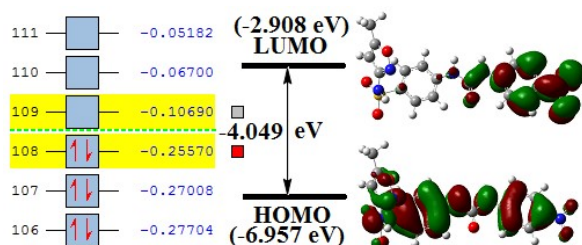




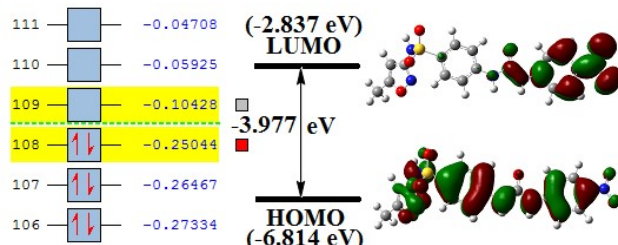
(c)



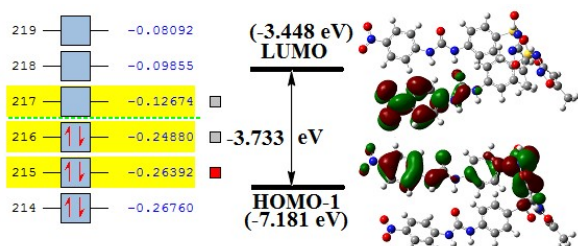
(d)



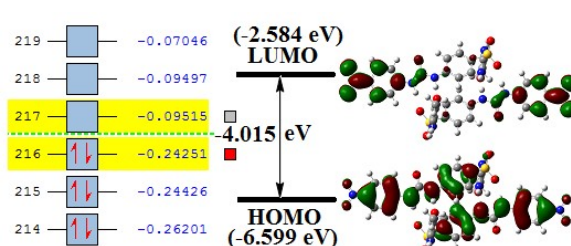
(e)



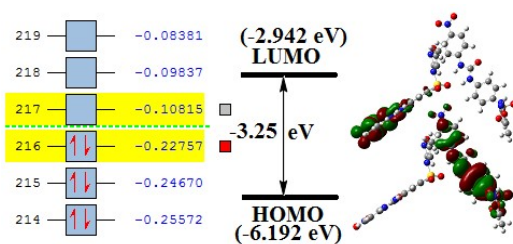
(f)



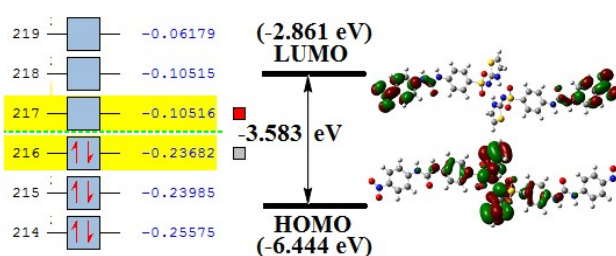
(g)



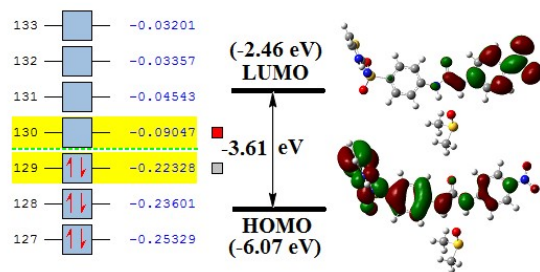
(h)



(i)



(j)



(k)

Figure S55: HOMO and LUMO gap in the (a) HSMZU.DMF-P1 (b) HSMZU.DMF-P2 (c) TBA(SMZU), (d) HSTZU.DMF (e) HSMZU-P1 (f) HSMZU-P2 (g) dimer of HSMZU-P1 (h) dimer of HSMZU-P2 (i) dimer of TBA(SMZU) (j) dimer of HSTZU.DMF (k) HSMZU.DMSO calculated by DFT using B3LYP/6-31+G (d, p) as basis set.